

The spectrum of light isovector mesons with $C = +1$ from the COMPASS experiment

Stephan PAUL
for the COMPASS collaboration

Physik Department, Technical University Munich, James Franck Str., 85748 Garching, Germany
email: *stephan.paul@tum.de*

September 30, 2016

Abstract

Based on the largest event sample of diffractively produced $\pi^-\pi^-\pi^+$, obtained by a pion beam of 190 GeV/ c momentum, the COMPASS collaboration has performed the so far most advanced partial-wave analysis on multi-body final states, using the isobar model. The large number of 88 waves included in the analysis reduces truncation effects. We have used fourteen waves, to extract resonance parameters for eleven light-meson candidates, most of them observed previously. The coherence of the analysis and the large variety of systematic studies has allowed us to determine mass and width of most a_J and π_J states with a total of six different values of J^{PC} below a mass of 2.1 GeV/ c^2 , with high confidence. We exploit that the production rates of resonant and non-resonant contributions in these fourteen waves vary differently with the four-momentum transfer squared in the reaction. In addition, we have performed the first isobar-freed analysis in diffraction, from which we have determined the shape of the $\pi\pi$ S -wave isobar for different J^{PC} of the 3π system.

Keywords: COMPASS, diffraction, hadron spectroscopy, partial-wave analysis, mesons, exotics, light quarks, isobar model, freed isobar

1 Introduction

The excitation spectrum of light-quark bound states has gained much interest in the last years. Recently, the simulation of QCD on the lattice has caught new momentum because it now also addresses the dynamics of meson decays, which will lead to more realistic predictions for masses and widths of excited hadrons. Thus, a precise knowledge of the spectrum of light hadrons has become important. Excited light-quark hadrons occur in the decay of heavy-quark mesons and are currently studied extensively in high-flux scattering experiments at CERN [1] and JLAB [2, 3]. At present, results from different experiments, summarized by the Particle Data Group (PDG) [4], vary considerably or even are inconsistent. Similarly, the interpretation of many states is controversial, as is the case e.g. for the new axial-vector state $a_1(1420)$ observed by COMPASS [5], which appears with the same quantum numbers as the elusive $a_1(1260)$ [6–10]. Mesons are characterized by their quantum numbers, isospin I and J^{PC} , with J being the total spin, P the parity and C the charge conjugation quantum number^[a]. Extensive discussions of the

^[a]Although the C parity is not defined for a charged system, it is customary to quote the J^{PC} quantum numbers of the corresponding neutral partner state in the isospin multiplet. The C parity can be generalized to the G parity $G \equiv C e^{i\pi I_y}$, a multiplicative quantum number, which is defined for the non-strange states of a meson multiplet.

light-meson sector are found in refs. [11, 12]. Here, we shall restrict ourselves to isovector states with assigned positive C parity and masses below about $2.1 \text{ GeV}/c^2$, decaying into $\pi^-\pi^-\pi^+$.

This work is based on the currently world's largest data of $50 \cdot 10^6$ events set on diffractively produced mesons decaying into $\pi^-\pi^-\pi^+$, which has previously been discussed in ref. [13].

2 Diffraction and Partial-Wave Analysis

2.1 Diffraction

Information on light hadrons can be obtained from heavy-meson decays and $\bar{p}p$ annihilations where they appear in subsystems of the measured final state and can be identified as interfering amplitudes in the Dalitz-plot. In diffractive production with incoming negatively charged pions, the beam particle is excited by the exchange of a Pomeron with the target nucleon or nucleus to form short-lived intermediate states X^- (see Fig. 1). The detection of the recoil proton suppresses events with inelastically scattered target particles. Still, more complex exchange processes may occur, which are not described by Fig. 1 but produce the same final state without passing through a resonance. These processes form a coherent background for resonance production and have to be singled out by other means. The decay of the states X^- proceeds independently of its production, which therefore factorize. The various X^- contributing coherently can be separated using partial-wave analysis (PWA).

2.2 Partial-wave analysis

For this, we employed the isobar model. It describes the transition of X^- into the final state (here $\pi^-\pi^-\pi^+$) as a sequence of two-body decays via additional intermediate states ξ , called isobars. The decays are represented by the vertices labeled 1 and 2 in Fig. 1. Both X^- and ξ are characterized by their quantum numbers J^{PC} . Together with the spin projection M of X^- and the reflectivity quantum number ϵ (see ref. [13]) it defines a wave, which represents a characteristic pattern in the five-dimensional phase space of the $\pi^-\pi^-\pi^+$ final state and also includes non-resonant processes. The full data set contains a mixture of coherent and incoherent contributions of various waves. These contributions (complex-valued production amplitudes) are extracted by an extended maximum likelihood fit. Such a fit is performed independently for individual bins of mass of the 3π final state $m_{3\pi}$, subdivided into bins in the reduced four-momentum transfer t' . The fits result in a spin-density matrix for each bin of mass and t' . A detailed description can be found in ref. [13]. Here, t' is defined by

$$t' \equiv |t| - |t|_{\min} \geq 0, \text{ where } |t|_{\min} \approx \left(\frac{m_{3\pi}^2 - m_\pi^2}{2|\vec{p}_{\text{beam}}|} \right)^2, \quad (1)$$

where t is the four-momentum transfer squared, m_π the pion mass and p_{beam} the beam momentum.

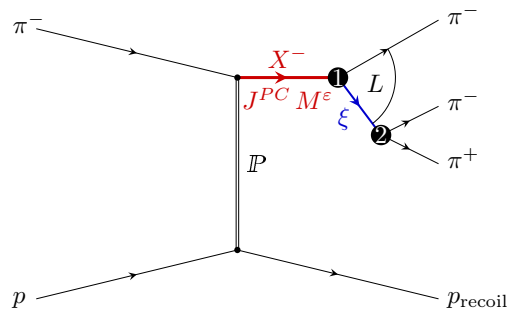


Figure 1: Diffractive production of X^- with quantum numbers J^{PC} and spin projection M , and naturality ϵ of the exchange particle. The decay is described in the isobar model and is assumed to proceed via an intermediate $\pi^-\pi^+$ state ξ , the so-called isobar. The relative orbital angular momentum of the isobar and the spectator pion is denoted by L .

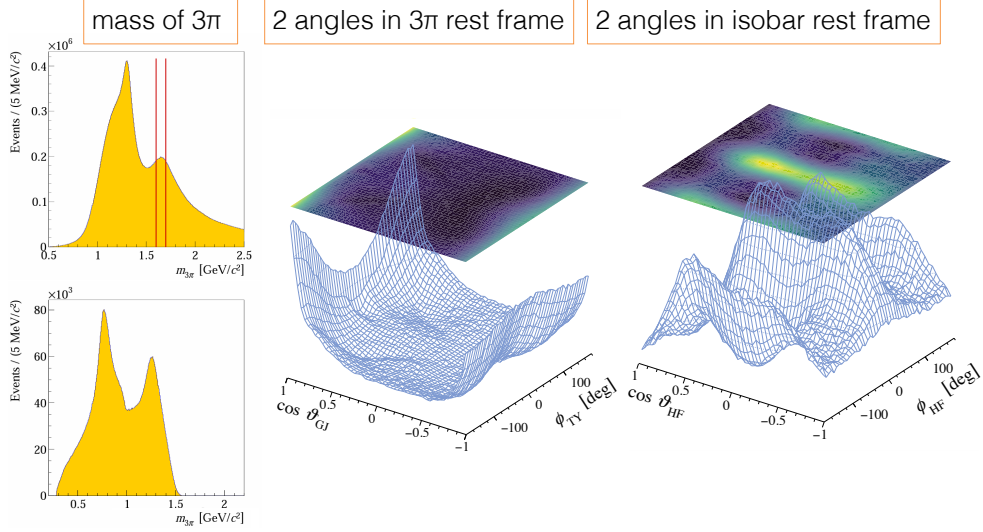


Figure 2: Kinematic distributions: spectrum of the invariant mass $m_{3\pi}$ of the final state (upper left); mass spectrum of the $\pi^+\pi^-$ subsystem (lower left) and the 2-body angular correlations in the Gottfried-Jackson frame (centre) and helicity frame (right), the latter three for $m_{3\pi} \in 1.6$ to $1.7 \text{ MeV}/c^2$.

Figure 2 shows some characteristic distributions for the $\pi^-\pi^-\pi^+$ final state: the spectrum of the final state mass $m_{3\pi}$, the mass distribution for the $\pi^-\pi^+$ subsystem for $m_{3\pi} \approx 1.6 \text{ GeV}/c^2$ and the corresponding angular distributions in the Gottfried-Jackson frame of X^- and the helicity frame of the isobar. The obvious dominance of isobars appearing in the $\pi^-\pi^+$ subsystem motivates the use of the isobar model in our analysis. The key issue of this first step the PWA analysis is the choice of waves forming a set. COMPASS has used the largest set ever, consisting of a coherent sum of 80 waves with positive reflectivity (natural parity exchange in the production process), a coherent sum of seven waves with negative reflectivity and one single incoherent wave representing pure phase space. About 97% of the total intensity can be described by waves with distinct isobaric character.

The result of this analysis is shown exemplarily in Fig. 3 for four prominent waves. The wave nomenclature follows $J^{PC}M^\epsilon[\text{isobar}]\pi L$. Each data point corresponds to the result of a single fit. We show the spectra for two bins of t' , the lowest bin of t' , $0.100 < t' < 0.113 (\text{GeV}/c)^2$, and the second highest one, $0.449 < t' < 0.724 (\text{GeV}/c)^2$. The spectra demonstrate the interplay of resonant and non-resonant components, whose production amplitudes exhibit different t' dependences. In particular, for the waves with $J^{PC} = 1^{++}$ and $J^{PC} = 2^{-+}$ the apparent peak position moves with t' , while the spectra for $J^{PC} = 2^{++}$ and $J^{PC} = 4^{++}$ show very little dependence on t' . This effect is independent of the charge combinations of the 3π final state, as is indicated for the case of $J^{PC} = 1^{++}$. Performing the partial-wave decomposition independently in narrow bins of t' allows us to better disentangle resonant and non-resonant amplitudes in the second analysis step (see Section 3).

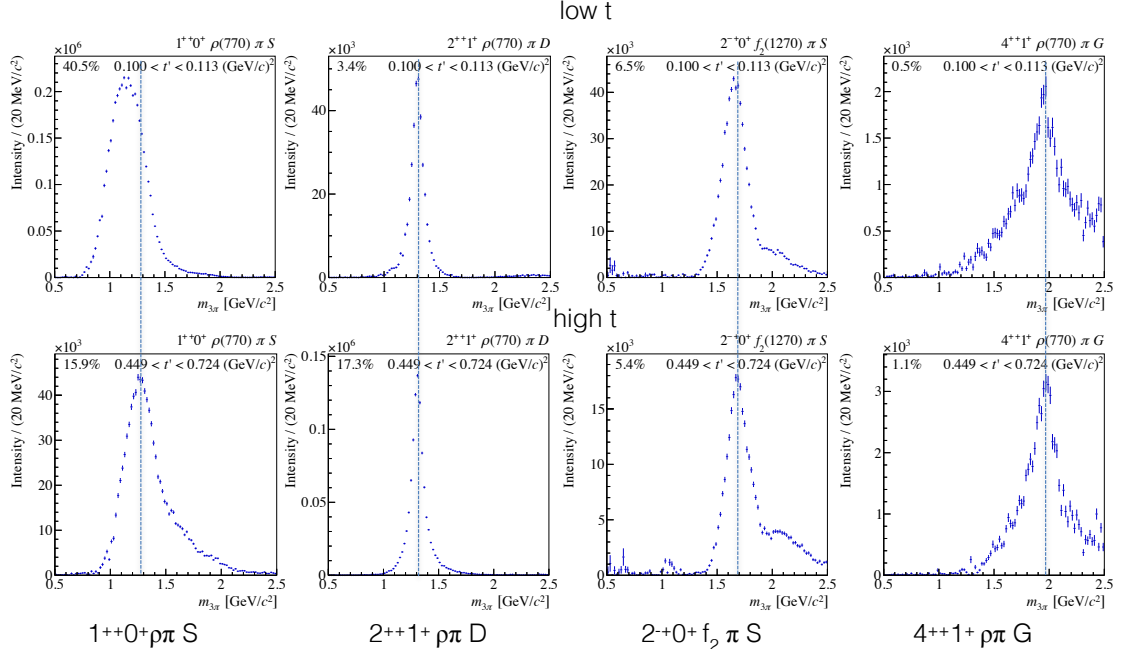


Figure 3: Intensity spectra for individual waves resulting from partial-wave fits. Each data point corresponds to the result of an independent fit. We show the spectra for two bins of t' (see text for details). Vertical lines are placed to guide the eye and indicate the intensity maximum for each wave at high values of t' . The fit fractions for the particular bin in t' are indicated for each wave.

3 Resonance-model fits

The steps described in Section 2.2 are the prerequisite to search for resonances produced in the reaction process, which can only be identified if we combine the information from all spin-density matrices over a wide range of final-state masses. For this step, different methods were used in the past. This includes K -matrix formalisms, where resonances are described by poles and the description of resonances by Breit-Wigner (BW) amplitudes. Here, we only treat one final state, namely $\pi^-\pi^-\pi^+$, and thus the full K matrix cannot be obtained from the data alone. In addition, the description of the non-resonant processes lacks a stringent recipe, and thus the fit model for this work consists of a sum of a set of BW amplitudes to describe resonances and a set of exponentials in the two-body break-up momentum for the background, separately. This technique was employed in previous analyses including our own work [5, 14]. The major extension of the number of waves allows to identify almost the complete isovector family with $C = +1$ at once and to determine systematic uncertainties in a consistent way. Theoretical and technical work necessary to implement K matrices is under development. The fit of the full spin density matrix composed of positive reflectivity waves only is technically very difficult owing to the large number of free parameters and requires a good modeling of the non-resonant contributions for all waves. Remaining artifacts from either the truncation of the partial-wave series or inherent to the isobar model render this task impractical and thus we have restricted our fits to only 14 waves listed in Table 1. We present and discuss the results in the following sections.

Figure 4 shows part of the spin-density submatrix used in the fit for one interval of t' . It relates the waves with $J^{PC} = 0^{-+}$ and 1^{++} to six of the other waves used. The fit model uses one relativistic BW each for 0^{-+} , 1^{-+} , 4^{++} and $1^{++} 0^{+} f_0(980) \pi P$, two BW for $1^{++} 0^{+} \rho(770) \pi S$ and $1^{++} 0^{+} f_2(1270) \pi D$ as well as $J^{PC} = 2^{++}$ and three BW for the three waves with $J^{PC} = 2^{-+}$. The non-resonant contributions are parametrized using exponentials of the same shape, with the exception of five waves for which the shape is t' dependent and modified by a power law. In order to avoid local maxima in the parameter space of the χ^2 function, we make 1000 fit attempts with randomly sampled starting values for the fit parameters and use different schemes for releasing and fixing of the parameters during the fit. Details of the fit procedure will be published soon in a dedicated paper.

Table 1: Waves used in the resonance-model fit

$0^{-+} 0^{+} f_0(980) \pi S$	$1^{-+} 1^{+} \rho(770) \pi P$
$1^{++} 0^{+} \rho(770) \pi S$	$1^{++} 0^{+} f_2(1270) \pi P$
$1^{++} 0^{+} f_0(980) \pi P$	$2^{++} 1^{+} f_2(1270) \pi P$
$2^{++} 2^{+} \rho(770) \pi D$	$2^{++} 1^{+} \rho(770) \pi D$
$2^{-+} 0^{+} f_2(1270) \pi S$	$2^{-+} 0^{+} f_2(1270) \pi D$
$2^{-+} 0^{+} \rho(770) \pi F$	$2^{-+} 1^{+} f_2(1270) \pi S$
$4^{++} 1^{+} \rho(770) \pi G$	$4^{++} 1^{+} f_2(1270) \pi F$

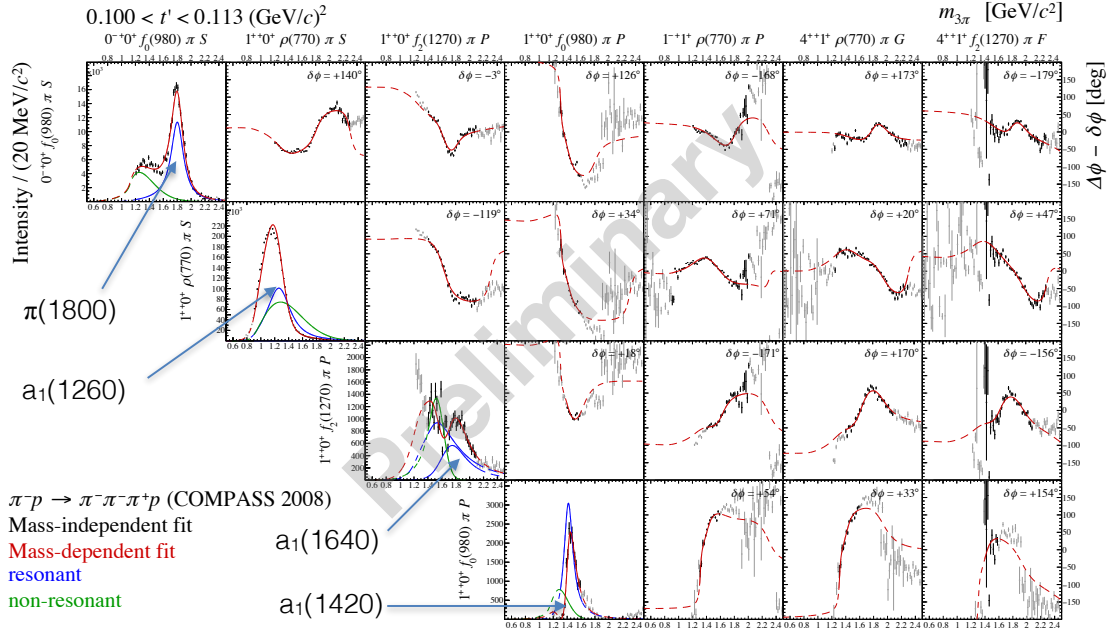


Figure 4: Submatrix of the full spin-density matrix obtained from the first step of our PWA. We show intensities for the $J^{PC} = 0^{-+}$ and 1^{++} waves used in our 14-wave fit, and the relative phases with respect to seven waves. The green curves represent the non-resonant contributions, the blue curves the resonances. The red solid lines represent the coherent sum of all contributions, the dotted part of the red line is the extrapolation into mass regions outside the fit range. The blue arrows point to resonances, assigned to the closest matching PDG entry [4].

3.1 Fit results

The results for all resonance are visualized in Fig. 5. For $J^{PC} = 1^{++}$, we observe three resonances. They appear with different relative strength in the various waves and thus allow a parametrization

in terms of BW resonances. The strong $1^{++} 0^+ \rho(770) \pi S$ wave contains a dominant structure around $1.2 \text{ GeV}/c^2$, which we decompose into a large non-resonant contribution and the $a_1(1260)$. This decomposition is supported by the different t' dependence of the components. However, there is no reliable interferometer at low masses, which would allow to observe the 180° phase variation of $a_1(1260)$. Thus, resonance parameters show large uncertainties, but we can rule out large values for the width of $a_1(1260)$ as reported by previous experiments. $a_1(1640)$ is hidden in this wave, but it becomes visible in the phase variation with respect to other waves and is distinctly observed in the spectral distribution of $1^{++} 0^+ f_2(1270) \pi P$. As this resonance appears in a mass region populated by many resonances with other J^{PC} , the extracted BW parameters are sensitive to choices in the analysis model. $a_1(1420)$ was previously unknown and could be unraveled in the $1^{++} 0^+ f_0(980) \pi P$ wave, despite its small production strength. The resonance parameters are very robust towards any systematic variations of analysis parameters. For $J^{PC} = 2^{++}$, we

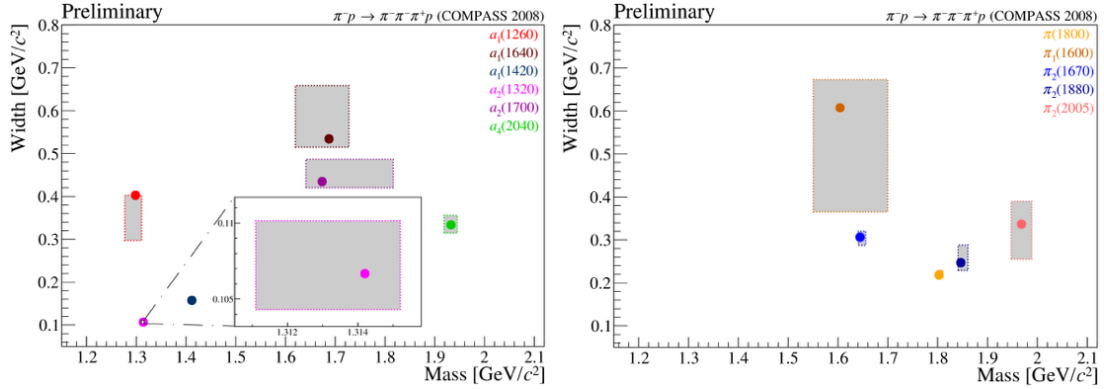


Figure 5: Results of the systematic studies for the resonance parameters of a_J states (left) and π_J states (right). The horizontal axes show the BW mass, the vertical axes the width of the BW. The size of the box indicates the systematic variations from a total of up to 20 systematic studies.

observe two states, $a_2(1320)$ and $a_2(1700)$. The latter exhibits strong interference effects with the non-resonant contribution in $2^{++} 1^+ \rho(770) \pi D$, which change from destructive to constructive as function of t' . The mass spectrum of $2^{++} 1^+ f_2(1270) \pi P$ shows a clear distinction of the two a_2 states. While the determination of the resonant parameters for $a_2(1320)$ is unambiguous, we observe large systematic uncertainties for $a_2(1700)$, owing to the large width of this state.

We observe three states with $J^{PC} = 2^{-+}$, which are relatively close in mass and have widths around 250 to 350 MeV/c^2 . Similarly to the a_1 sector, these resonances appear in the various waves with different strength. The $2^{-+} 0^+ f_2(1270) \pi S$ and $2^{-+} 1^+ f_2(1270) \pi S$ waves are dominated by $\pi_2(1670)$, which, however, is very weak in $2^{-+} 0^+ f_2(1270) \pi D$. The latter wave in turn is dominated by $\pi_2(1880)$ with a smaller contribution of $\pi_2(2005)$. The wave $2^{-+} 0^+ \rho(770) \pi F$ shows a clear signal for $\pi_2(2005)$, in particular at large values of t' . Also $\pi_2(1670)$ appears here, while $\pi_2(1880)$ plays a minor role. We conclude from our analysis that $\pi_2(1880)$ is an independent state and thus disfavor the suggestions of it being a reflection of $\pi_2(1670)$ interfering with non-resonant contributions [15]. Our systematic studies reveal correlations in the determination of BW parameters for the two excited π_2 .

The spin-exotic state $\pi_1(1600)$ is hidden beneath a large non-resonant contribution at small values of t' . However, similarly to $a_1(1260)$, it can be singled out at our largest values of t' . While the determination of the mass of $\pi_1(1600)$ is rather robust, the value for the width extracted from the various fits reveals large uncertainties, mostly connected to the sector of $J^{PC} = 1^{++}$.

The exotic $\pi_1(1600)$ appears wider than previously observed. For $J^{PC} = 0^{-+}$ and 4^{++} , we observe the well known states $\pi(1800)$ and $a_4(2040)$ and determine the resonance parameters with very small systematic uncertainties. The values for mass and width are consistent with previous observations, however, $a_4(2040)$ is slightly lighter than determined by ref. [4], using several previous measurements.

The separation of various components within all waves has strongly profited from their different t' -dependent production rates. We have integrated their contributions over $m_{3\pi}$ and the resulting t' dependence has been described by a single exponential multiplied by $t'^{|M|}$, with M being the spin projection quantum number. The result is shown exemplarily for $J^{PC} = 1^{++}$ in Fig. 6. The slope parameter b of the exponential shows some regular patterns, although with some exceptions. In general, the slope of the t' dependence flattens with increasing mass of a resonance within a particular J^{PC} . Most values for b are in the range of 6 to 9 $(\text{GeV}/c)^{-2}$ for resonances and non-resonant contributions often drop much faster than the resonant ones. Some exceptions are the slope parameter for $a_1(1260)$ of $b = 12.7 (\text{GeV}/c)^{-2}$ or the very shallow slopes for the non-resonant contributions for $J^{PC} = 2^{-+}$, where these non-resonant contributions are small and we fit with three BW functions. Similar is true for $J^{PC} = 2^{++}$, where again the non-resonant contributions are small and may not be fully separated from the resonant ones.

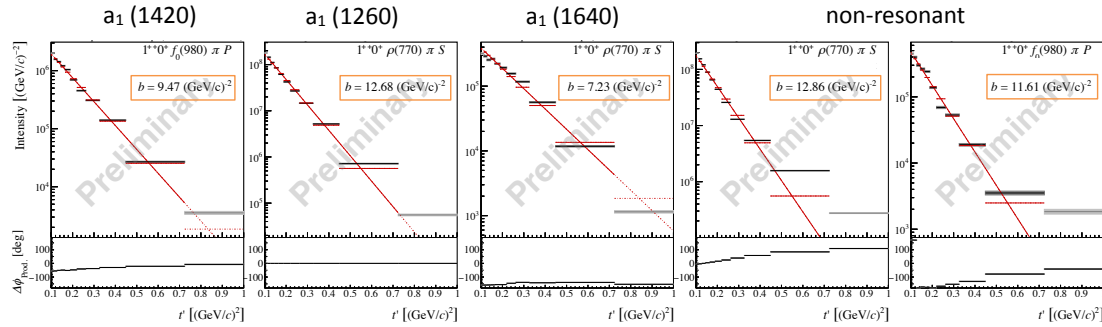


Figure 6: t' dependence of the integrated yield for the different fit components for $J^{PC} = 1^{++}$ (upper row). t' dependence of the production phase with respect to $a_1(1260)$ for the different components (lower row).

4 Freed-Isobar Analysis

The conventional isobar model implies that final-state interaction does not alter the shape of the isobars, which are implemented with a fixed shape taken from ref. [4] or, for the $\pi\pi$ S -wave, from $\pi\pi$ scattering data. In order to test this hypothesis, we have replaced the fixed parametrization of $\pi\pi$ S -wave by a series of step-like functions across the $\pi^-\pi^+$ mass spectrum, individually for each bin of $m_{3\pi}$. Owing to the large increase in the number of free parameters, we have restricted this exercise to only three values of J^{PC} for $\pi^-\pi^-\pi^+$ with $\pi\pi$ S -wave isobar, namely 0^{-+} , 1^{++} and 2^{-+} .

The result is a correlation of the spectral distribution of the $\pi^-\pi^+$ system with $J^{PC} = 0^{++}$ and the corresponding $m_{3\pi}$ spectrum with definite J^{PC} . Figure 7a shows the result for the 0^{-+} system. As we extract the complex amplitude for the $\pi^-\pi^+$, we present in Figure 7b the mass dependence of real and imaginary part in an Argand diagram for a $m_{3\pi}$ interval around $\pi(1800)$. With increasing $m_{\pi^-\pi^+}$, the function forms two full circles, which correspond to the $f_0(980)$ and $f_0(1500)$ isocalars. Thus, the coupling of $\pi(1800)$ to both isoscalars can directly be deduced. In

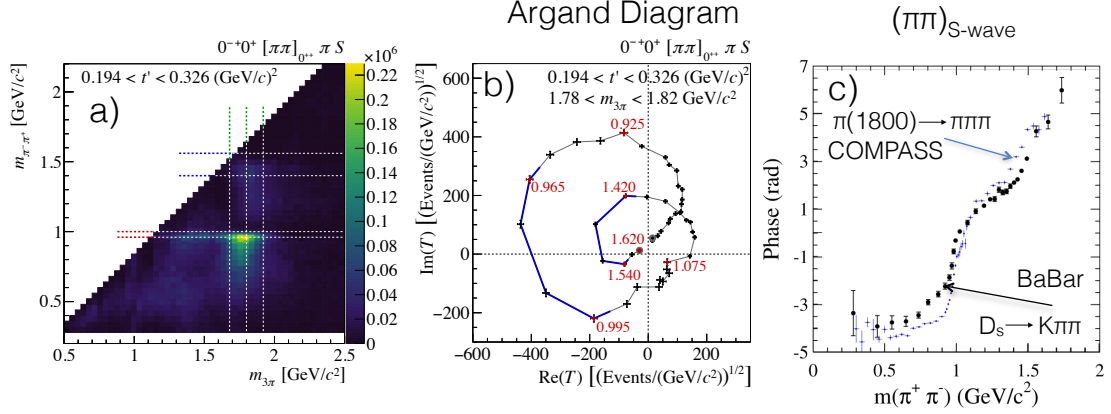


Figure 7: Results from a freed-isobar PWA. a) $m_{\pi^-\pi^+}$ in 0^{++} vs. $m_{3\pi}$ in 0^{-+} for one bin in t' ; b) Argand diagram for the corresponding $\pi^-\pi^+$ amplitude selecting $m_{3\pi}$ around the mass of $\pi(1800)$. Red labels indicate $m_{\pi^-\pi^+}$ along the trajectory; c) comparison of the $\pi\pi$ S -wave in three body decays from D_s (Babar [16]) and $\pi(1800)$ from this analysis.

order to examine the result, we compare the corresponding phase of $\pi^-\pi^+$ (measured with respect to $1^{++}0^+ \rho(770) \pi S$) to an analog analysis using decays of $D_s \rightarrow K\pi\pi$ from Babar [16], shown in Figure 7c. To help the comparison, we use an arbitrary phase offset for our data. We can deduce that the phase of the $\pi\pi$ S -wave shows a similar behaviour, whether originating from the three-body weak decay of D_s mesons or from the strong decay of $\pi(1800)$, itself extracted by means of PWA from our data.

5 Conclusion

COMPASS has performed a two-step PWA on a data set comprising about $50 \cdot 10^6$ events in the $\pi^-\pi^-\pi^+$ final state, using the so far largest model space with 88 waves. We have extracted resonance parameters for eleven isovector mesons with $C = +1$. The analysis revealed a new $a_1(1420)$, the nature of which is much debated in the literature. We have confirmed the existence of three different π_2 states as well as $\pi_1(1600)$. The width of $\pi_1(1600)$ is considerably larger than previous observations, although systematic uncertainties are large. Also $a_1(1640)$ and $a_2(1700)$ have well been identified, though resonance parameters are still uncertain. This work constitutes the first coherent observation of all these states within one analysis. This allowed to study a large variety of systematic uncertainties for the resonance parameters connected to wave selection and model variation in these fits.

References

- [1] P. Abbon et al. The COMPASS setup for physics with hadron beams. *Nucl. Instrum. Methods Phys. Res., Sect. A*, 779:69–115, 2015.
- [2] M. Battaglieri. Present and future of hadron spectroscopy at Jefferson Lab. *Int. J. Mod. Phys.*, E19:837–843, 2010.

- [3] H. Al Ghouli et al. First Results from The GlueX Experiment. In 16th International Conference on Hadron Spectroscopy (Hadron 2015) Newport News, Virginia, USA, September 2015.
- [4] K. A. Olive et al. Review of Particle Physics. Chin. Phys. C, 38:090001, 2014.
- [5] C. Adolph et al. Observation of a New Narrow Axial-Vector Meson $a_1(1420)$. Phys. Rev. Lett., 115(8):082001, 2015.
- [6] F. Aceti, L. R. Dai, and E. Oset. The " $a_1(1420)$ " peak as the $\pi f_0(980)$ decay mode of the $a_1(1260)$. 2016.
- [7] Wei Wang and Zhen-Xing Zhao. Production of a_1 in heavy meson decays. Eur. Phys. J., C76(2):59, 2016.
- [8] Hua-Xing Chen, Er-Liang Cui, Wei Chen, T. G. Steele, Xiang Liu, and Shi-Lin Zhu. $a_1(1420)$ resonance as a tetraquark state and its isospin partner. Phys. Rev., D91:094022, 2015.
- [9] M. Mikhasenko, B. Ketzer, and Andrey Sarantsev. Nature of the $a_1(1420)$. Phys. Rev. D, 91(9):094015, 2015.
- [10] Zhi-Gang Wang. Light axial-vector tetraquark state candidate: $a_1(1420)$. 2014.
- [11] Eberhard Klempt and Alexander Zaitsev. Glueballs, hybrids, multiquarks: Experimental facts versus QCD inspired concepts. Phys. Rep., 454:1–202, 2007.
- [12] N. Brambilla, S. Eidelman, P. Foka, S. Gardner, A. S. Kronfeld, et al. QCD and strongly coupled gauge theories: challenges and perspectives. Eur. Phys. J. C, 74(10):2981, 2014.
- [13] C Adolph et al. Resonance Production and $\pi\pi$ S-wave in $\pi^- + p \rightarrow \pi^- \pi^- \pi^+ + p_{recoil}$ at 190 GeV/c. submitted to Phys. Rev. D, 2015.
- [14] M. Alekseev et al. Observation of a $J^{PC} = 1^{-+}$ Exotic Resonance in Diffractive Dissociation of 190 GeV/c π^- into $\pi^- \pi^- \pi^+$. Phys. Rev. Lett., 104:241803, 2010.
- [15] J. Dudek and A. Szczepaniak. The Deck effect in $\pi N \rightarrow \pi\pi\pi N$. AIP Conf. Proc., 814:587–591, 2006.
- [16] Bernard Aubert et al. Dalitz plot analysis of $D_s^+ \rightarrow \pi^+ \pi^- \pi^+$. Phys. Rev. D, 79:032003, 2009.